Meteotsunami Events and Hydrologic Response in an Isolated Wetland: Beaver Island in Lake Michigan, USA

Wendy M. Robertson[1,2], Daria B. Kluver[1,2], John T. Allen[1,2], and Eric J. Anderson[3]

[1]Central Michigan University Department of Earth and Atmospheric Sciences.

[2]Central Michigan University Institute for Great Lakes Research.

[3]Colorado School of Mines Hydrologic Science and Engineering Program, Department of Civil and Environmental Engineering

Corresponding author: Wendy M. Robertson (rober2w@cmich.edu)

Key Points:

- We documented and described hydrologic response to a meteotsunami event in an isolated wetland
- Atmospheric bores may lead to meteotsunamis that are remote of the convective forcing.
- Existing meteotsunami detection methods can't be applied to isolated wetland records because the hydrologic response is non-symmetric

Abstract

Meteotsunamis are both a well-known and poorly understood phenomenon. In particular, the influence of and disturbance by meteotsunami on coastal wetlands is largely unknown. This paper documents a case illustrating how water levels in an isolated wetland, specifically an incipient foredune/swale complex, in northern Lake Michigan responded to a meteotsunami event. We identified potential meteotsunami influence on wetland water levels through slope-break analysis, verified the presence of meteotsunami waves at surrounding lake water level gauge stations with wavelet analysis, analyzed both regional and small-scale meteorological data to establish what source of atmospheric forcing resulted in meteotsunami formation, and used a hydrodynamic model to simulate lake surface response and meteotsunami generation. Here, we present what we hypothesize reflects an idealized response of wetland water levels to meteotsunami influence where an atmospheric bore propagating away from a convective system formed a meteotsunami event that was captured in subsurface water levels beneath the isolated wetland. While this event produced an obvious response, the potential for multiple sources of meteorological forcing and secondary wave refraction highlights several of the challenges with predicting generation of and hazard from meteotsunami events. These issues equally translate in how the current methodology can be applied to isolated wetland systems. The event presented in this study make a strong case for focused research on coastal wetland response to meteotsunamis (and meteotsunami-like events) to address this understudied impact given its implications for coastal processes and resiliency.

Plain Language Summary

While scientists are learning more about meteorological tsunamis (‘meteotsunamis’) so we can predict what causes them and where they might strike, we know less about how meteotsunamis affect wetlands, especially wetlands that aren’t directly connected to a body of water (‘isolated wetlands’). This is important because wetlands often act as the first line of defense, helping to protect coastlines from wave damage. We looked at how water levels in an isolated wetland on an island in Lake Michigan changed when the bay where the wetland was located was hit by meteotsunamis. We found that weather events that happen further away from where we would predict can produce meteotsunamis big enough to change wetland water levels and the way that the water levels change in isolated wetlands after being hit by a meteotsunami looks different from a meteotsunami wave in an open body of water which suggests we need to develop new ways to identify these waves. Future research needs to move beyond deadly or destructive meteotsunamis so that we can effectively predict potential causes and hazards of these events and make informed decisions about how to manage coastal wetlands.

1 Introduction

Meteorological tsunamis (or meteotsunamis) are traveling water waves with the same periodicity (~2-120 min) as tsunami waves generated by tectonic processes (e.g., earthquakes, volcanic eruptions, and landslides) but are instead caused by atmospheric disturbances (Nomitsu, 1935; Monserrat et al. 2006; Rabinovich et al. 2006; Dusek et al. 2019; Anarde et al. 2021 and others). Meteotsunamis have been widely observed on the coasts of ocean basins and seas around the globe and in the U.S. Great Lakes (Vilbic et al. 2016; Dusek et al. 2019; Vilbic et al. 2021). While the amplitudes of meteotsunamis are generally smaller and their effects more localized than the more widely known tectonically generated tsunamis, they still pose considerable danger

and can be destructive under the right conditions (Bechle and Wu, 2014; Dusek et al. 2019; Vilbic et al. 2021). Additionally, the disturbances that generate meteotsunamis (e.g., atmospheric gravity waves, cyclones, thunderstorms, mesoscale convection, etc.) are common, making it likely that these kinds of tsunamis occur more frequently than their tectonically driven counterparts (ten Brink et al. 2014; Bechle et al. 2016; Angove et al. 2021; Vilbic et al. 2021; Williams et al. 2021, Anderson and Mann 2021), especially in places like the U.S. Great Lakes region which has low exposure to tectonic hazards.

The U.S. Great Lakes have a long and well-known history as a meteotsunami 'hotspot' where the phenomena are frequent, often destructive, and sometimes fatal (Ewing et al. 1954; Platzman, 1958; Bechle and Wu, 2014; Anderson et al. 2015; Bechle et al. 2015, 2016; Matheny, 2017; Linares et al. 2019; Angove et al. 2021; Gusiakov, 2021 and others). Until recent work by Bechle et al. (2016) and others, meteotsunami occurrence was under-reported and likely biased towards heavily populated regions as documentation of the phenomena relied on eye-witness accounts (Bechle et al. 2016). Within the U.S. Great Lakes, the most frequent and largest meteotsunami events tend to occur in Lake Michigan (with an average of 51 events per year; Bechle et al. 2016); these findings are consistent with frequency of convective storm events and the presence of bathymetry favorable to meteotsunami initiation, amplification, and transformation (Pattiaratchi and Wijeratne 2015; Bechle et al. 2016; Linares et al. 2018).

Climatologically, the Great Lakes are an ideal region for atmospheric conditions that initiate meteotsunamis, particularly due to the favorable moisture and stability conditions, preferential cyclone track, and jetstream position. The region experiences enhanced convection, peaking in mid-summer (Kelly and Schaefer, 1985, Haberlie and Ashley 2019, Taszarek et al. 2020a), and frontal zone forcing of convection (Sanders and Hoffman 2002, Lagerquist et al. 2020), which occurs in late spring through summer. In the later summer months, there is also regular initiation of convection through lake breezes (Laird et al. 2001). These conditions contribute to the regular formation of organized and severe storms across the region (Haberlie and Ashley 2019, Taszarek et al. 2020b) which research identifies as the primary atmospheric driver of meteotsunami events on Lake Michigan (78%; Bechle et al. 2015; Bechle et al. 2016). Potential drivers for the regularity of meteotsunamis associated with these mesoscale systems include both wind and pressure sources, while generated atmospheric gravity waves driven by strong barometric pressure changes have also been suggested (Bechle et al. 2016; Anderson and Mann 2021)

Systematic observation, prediction, and risk assessment of meteotsunami hazard is a relatively new but growing field of research. One area in which there has been limited investigation is the disturbance by, and response to, meteotsunami events along the open coast; i.e., coastlines unprotected from open water. To date, most of the long-term record relies on tidal and water level observation stations in harbors and bays (Bechle et al. 2015; Vilbic et al. 2016; Anarde et al. 2021). While the meteotsunami threat to lives and infrastructure in more built-up areas (e.g., harbors, coastal cities) is potentially large and devastating, the scientific and policy communities should not ignore the role that meteotsunamis may play in coastal geomorphological processes, hydrologic budgets, ecosystem disturbance, and resilience of open coast systems. The effects and interactions that meteotsunami events have on wetlands is largely undocumented, despite the scientific consensus surrounding the importance of wetlands for maintaining biodiversity, mitigating coastal flooding, regulating sediment supply and transport,

and providing other key ecosystem services (e.g., Zedler and Kercher 2005; Barbier, 2013; Curreli et al. 2013; Gracia et al. 2018).

The purpose of this paper is to document meteotsunami influence and hydrologic response of an isolated wetland, specifically an incipient foredune/swale wetland complex, located on the Beaver Island Archipelago in northern Lake Michigan. To our knowledge, this is the first study to document and portray meteotsunami influence in the hydrologic record of an isolated wetland system. Focusing on one case from July 20th, 2019, we evaluate the meteorological conditions that drove meteotsunami formation, identify meteotsunami occurrence in lake level records coincident to the observed changes in wetland water levels, use a hydrodynamic model of water surface response to identify meteotsunami generation and describe the influence of meteotsunami waves on the wetland. We then discuss some of the challenges and limitations, including differentiation between meteotsunami influence and other wave action in wetland water levels, the spatially disparate and diverse meteorological phenomena that can drive meteotsunami formation, and the drawbacks to prior methodologies that can result in event aggregation. Finally, we discuss the implications of our findings and highlight some avenues for future research to improve our understanding of the role of meteotsunamis in open coast systems.

2 Study Site

The 14 islands of the Beaver Island Archipelago (BIA) are situated in northern Lake Michigan (Figure 1). North of the deepest part of Lake Michigan (the Chippewa Basin), which reaches depths of greater than 250 m, the water surrounding the archipelago is generally shallow (< 50 m; National Geophysical Data Center, 1996). Beaver Island (BI; 145 km^2), is the largest and the only island within the archipelago with a year-round population; it is located approximately 50 km from Charlevoix, MI. Sand Bay, on the eastern side of BI (Fig. 1c, d), is south of the BI harbor in Peaine Township. The bay has an average lake slope of 0.004-0.008 (National Geophysical Data Center, 1996). Central Michigan University maintains a Biological

Station (CMUBS) in Sand Bay; on this property are a series of incipient foredune/swale wetland complexes located along the shoreline of Lake Michigan (Figure 1D).

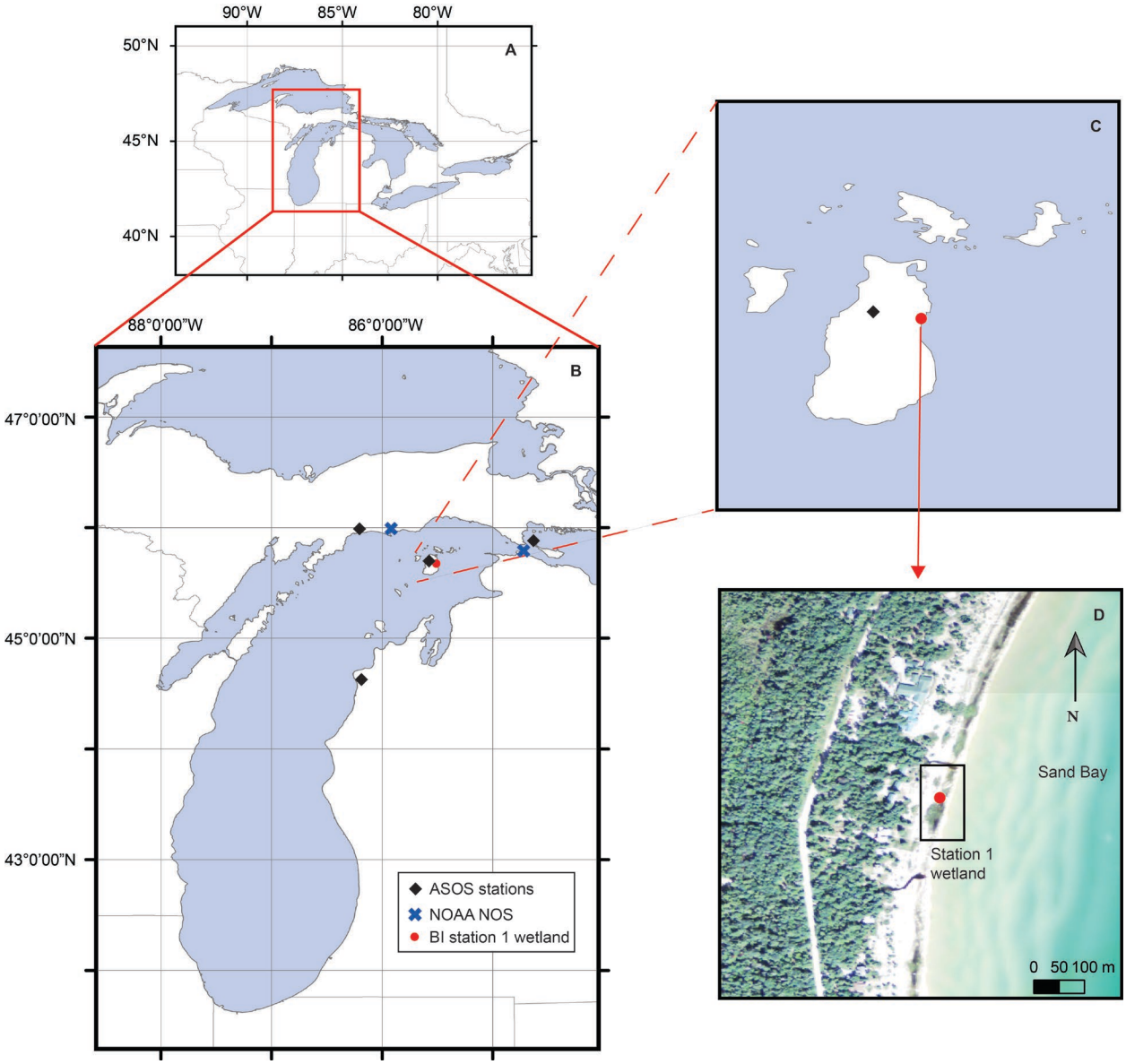

Figure 1. Map of study area with (a) regional setting, (b) Lake Michigan and locations of BI station 1, ASOS stations used for wind analysis (Manistique (ISQ), Beaver Island (SJX) Mackinaw Island (MCD), and Frankfort (FKS)), and NOAA NOS water level observation stations at Port Inland (station ID 9087096) and Mackinaw City (station ID 9075080) Michigan, (c) BI, BI ASOS station, and BI station 1 wetland, and (d) aerial imagery of the station 1

incipient foredune/wetland complex. Aerial imagery from the USDA National Agriculture Imagery Program (NAIP; USDA-FSA-APFO Aerial Photography Field Office, 2014).

The surficial geology of BI is dominated by lacustrine sands and gravels, with the bedrock formations comprised of Devonian-aged sandstone and limestones (DeBois fm. and Detroit River group; Farrand and Bell, 1982; Michigan Department of Environmental Quality, 1987). The long axis of the incipient swale wetlands runs N-NE to S-SW (Fig. 1d) with the incipient foredunes located ~10 m from the water line in 2016 and ~5 m from the water line in 2020. Fluctuating lake levels and wind erosion have led to transgression and foredune migration during the past decade; the shoreline has receded approximately 35 m inland between 2010 and 2020 (USDA-FSA-APFO Aerial Photography Field Office 2010, 2020). Water levels in and beneath the station 1 wetland fluctuate rapidly in response to changes in lake level. No surface inflows are present; however, the swales remain saturated with water above or near (< 10 cm) the sediment surface year-round. Foredune/swale vegetation is dominated by dune grasses (sp. *Ammophila breviligulata* and *Agropyron dasystachyum*), with some sedge species (*Eleocharis*) and perennial flowering plants (*Potentilla anserine*; Girdler and Barrie, 2008).

3 Methods

3.1 Analysis and identification of meteotsunami events from wetland data

In August 2016, the station 1 wetland was outfitted with a hydrometeorological station to monitor and record windspeed (ms^{-1}), precipitation (mm), barometric pressure (kPa), air temperature (°C), relative humidity (%), shallow ground temperature (10 cm; °C) and moisture (10 cm; m^3/m^3), groundwater level (m asl) at two depths (0.5 and 0.75 m below ground surface), and wetland surface water level (m asl) at 15-min intervals. Data collection continued through June 2020. There is a complete record between 08/08/2016 and 06/22/2020 for all observations except wetland surface water level; wind, wave, and ice action repeatedly displaced the wetland stilling well, resulting in extensive record gaps between December 2016 andSeptember 2019. We recorded wellhead elevation of the groundwater piezometers and stilling well (wetland water level) at the time of installation using the Theodolite app (Hunter Research and Technology, LLC) and compared them to the U.S. Geological Survey one meter DEM (U.S. Geological Survey, 2020) plus measured stick-up height to verify their precision. To produce water levels in meters above sea level (m asl) we corrected the observed water levels using barometric compensation and wellhead elevations.

We identified instances of potential meteotsunami influence on the station 1 wetland by examining changes in the wetland water level records. We hypothesized that when a meteotsunami wave interacts with an isolated wetland, either through surface inundation or pressure wave propagation in the subsurface, the response of wetland water levels should be rapid and larger than could be accounted for from other inputs (e.g., direct precipitation). Therefore, we used rising limb slope characteristics and event magnitude from baseline to peak to identify potential instances of meteotsunami influence. Periodic sharp (< 4 hour from baseline to peak) and large (> 15 cm) increases in water level occurred in both the groundwater and wetland surface water levels that could not be explained by input from precipitation. Of the numerous (>20) documented events, this study focuses on one in particular; July 20th, 2019. This case represents what we hypothesize is close to the idealized response of water levels in an

incipient foredune/swale wetland to being struck by a single meteotsunami wave with no influence from storm surge, seiche, or subsequent refracted secondary meteotsunami waves. The peak water level during this event (178.1 masl) exceeded the 99th percentile of water level observations for both 2019 and the period of record (2016-2020), making it one of the largest water level fluctuations observed in this timeframe (SI Table 1).

3.2 Analysis and identification of meteotsunami events from Great Lakes water level data

To confirm meteotsunami event occurrence in northern Lake Michigan during the same window as the sharp fluctuations in station 1 wetland water levels, we used the National Oceanic and Atmospheric Administration (NOAA) National Observation Station (NOS) water level data at Port Inland, MI (9087096) and Mackinaw City, MI (9075080; https://tidesandcurrents.noaa.gov/stations.html?type=Water+Levels; Fig. 1). As with several previous studies that identify Great Lakes meteotsunami events, we examined water level data within the tsunami frequency band (2 – 120 min; Monserrat et al. 2006; Bechle et al. 2015; Bechle et al. 2016; Linares et al. 2016) using wavelet analysis, which is an ideal method for documenting the occurrence of meteotsunamis because it decomposes spectral characteristics over time. This approach is particularly useful for non-stationary wave patterns such as meteotsunami (Torrence and Compo, 1998; Pattiaratchi and Wijeratne, 2014; Dusek et al. 2019). Through the shifting and scaling of the mother wavelet, we can identify low through high frequency time series components at specific times, which is an advantage over Fourier transforms that assume stationary wave patterns.

Before performing the wavelet analysis, we prepared the water level data by detrending using a polynomial regression (loess smoother), and standardizing (z-score; Roesch and Schmidbauer 2018) it. We quantified wavelet energy through time by applying a continuous wavelet transform using a Morlet mother wavelet. Due to the Nyquist frequency associated with 6-minute NOS water level observations, meteotsunami were only detectable with periods of 12 minutes and higher. We calculated peak wavelet energy to identify energy signatures with periods from 12 to 120 minutes. We present the results of the wavelet analysis in terms of wavelet power spectrum (square of the amplitude) in the time-period domain (Carmona et al.1998; Torrence and Compo, 1998; Duske et al. 2019; Roesch and Schmidbauer 2018). We calculated mean wavelet power at each station for the period between 8/7/2016 and 6/22/2020 so the window of analysis would be consistent with station 1 wetland data availability. We defined a threshold of 6 standard deviations from the mean wavelet power to determine the presence of meteotsunami waves, henceforward denoted as ‘sigma’. This threshold is consistent with previous research where the thresholds were 4* and 6*sigma (Monserrat et al. 2006; Dusek et al. 2019).

3.3 Analysis and identification of meteotsunami events from atmospheric data

We assessed the presence of gust fronts or outflow boundaries that can potentially cause meteotsunamis using 5-minute NOAA Automated Surface Observing System (ASOS) data retrieved from the Iowa Environmental Mesonet site (https://mesonet.agron.iastate.edu/request/download.phtml) at four Michigan stations: Beaver Island (SJX), Manistique (ISQ), Frankfort (FKS) and Mackinaw Island (MCD; Figure 1). Wind

measurements for ASOS stations follow the standard procedure of calculation from 1-second measurements, and averages calculated over 5-second periods, with direction calculated to the nearest degree and wind speed to the nearest knot. From these, we calculated 2-minute averages that represent raw wind output. Wind gusts are based on the greatest 5-second average wind speed and direction in any 10-minute period and are retained only where wind is non-zero and exceeds the 2-minute average by at least 3 knots (National Oceanic and Atmospheric Association, 1998). The minimum reportable strength of gust is 14 knots. However, it should be noted that identification of wind shifts is a known limitation of ASOS stations and can lag by up to 15 minutes. Also, wind speed measurements on ASOS stations have an accuracy of ±2 knots or 5% (whichever is greater), while wind directions are accurate to ±5 degrees.

We also used temperature measurements to identify the character of the atmospheric feature generating each meteotsunami event. In the operating range for these two cases, resolution is to the nearest 0.1°F with a root-mean-squared error of 1.1-4.7°F. We calculated station barometric pressure (hPa) using the Metpy package and leveraging the raw data from the ASOS station altimeter and elevation, applying the conversion factors described in Smithsonian (1951) and assuming a standard atmosphere (NOAA 1976). For both ASOS measurements, a slope break analysis was used to identify the period of interest that corresponds to meteotsunami generation.

To identify the period during which storms were present over Lake Michigan and characterize their morphology, we used National Weather Service Doppler Radar in the form of the composite gridded synthesis product GridRad (Homeyer et al. 2017). We sourced data for the 20-22nd July 2019 case from the GridRad archive (Bowman et al. 2017) fdirectly from the dataset creator (Homeyer, Pers. Comm. 2021) . This provided 5 minute data and included dual-polarization products in v4.0. GridRad data are a fully 3D weighted blending of the individual radar sites.Owing to the distance of northern Lake Michigan from the respective radar sites, dual-polarization coverage is limited due to beam height, therefore, we focused on analyzing reflectivity only to infer storm position and structure. To synthesize the data to a single level, we calculated maximum column reflectivity for each radar grid and filtered using a 20 dBZ minimum threshold to remove clutter and noise. We performed radar analysis for the period 0245-0500UTC for the 20th of July 2019. In lieu of showing all individual radar scans, we used the leading edge of high reflectivity (>35 dBZ) as an indicator of position of the bow echo gust front..

3.4 Hydrodynamic modeling of the meteotsunami event

To supplement the analysis of observed water level and atmospheric data during the July 20th, 2019 event, we used a hydrodynamic model to simulate the water surface response and help in identification of meteotsunami generation. The model is based on the Finite Volume Community Ocean Model (FVCOM; Chen et al., 2006), which has been adapted for freshwater and successfully implemented for Great Lakes meteotsunami simulation (Anderson and Mann, 2021; Anderson et al., 2015; Huang et al., 2021) and other physical processes (Anderson and Schwab, 2013, 2017; Anderson et al., 2018). The model uses an unstructured grid with horizontal resolution that ranges from 100 m in the nearshore to 2500 m in offshore regions. For this event, the model was initialized at 00 GMT on July 20, 2019, from conditions taken from the National Oceanic and Atmospheric Administration (NOAA) Lake Michigan-Huron Operational

Forecast System (LMHOFS; Peng et al., 2019), which is a real-time operational implementation of the model configuration described in *Anderson and Mann, (2021)*. The event was simulated using 15-minute meteorological forcing (2-m air pressure, 10-m meridional and zonal wind, 2-m air temperature, 2-m humidity, and downward solar radiation) from the 00 GMT forecast on July 20, 2019, of the NOAA High-Resolution Rapid Refresh (HRRR; Benjamin et al., 2016) version 3, which has been employed to successfully simulate meteotsunami generation for past events on Lake Michigan (Anderson and Mann, 2021; Huang et al., 2021). Pressure was adjusted to MSLP as required by FVCOM using the hypsometric relationship (Smithsonian 1951) and assuming a standard atmosphere (NOAA 1976), while other variables were used in their native formats. Although meteotsunami events are typically simulated with higher frequency atmospheric conditions for mesoscale convective events (e.g., 5-minute), 15-minute data was the highest temporal resolution data available for the time-period of study. Forecast data was used as opposed to analysis data to avoid discontinuities arising from the assimilation of observations in the forcing. Output from the hydrodynamic model was produced every 2 minutes to resolve wave conditions in the meteotsunami frequency band.

4 Results

The July 20th, 2019, case exhibits what we expect might be idealized response of an isolated wetland to a meteotsunami wave influence. This case illustrates how a wetland-influencing meteotsunami appears for a simple scenario where an incipient foredune/swale wetland is struck by a meteotsunami wave without any influence from additional refracted waves, seiche, or storm surge. The atmospheric conditions that preceded meteotsunami formation over Lake Michigan were characterized by a nocturnally stable marine atmospheric boundary layer, with capping inversion evident in sounding data from Green Bay, Wisconsin at 00:00 UTC on July 20th (not shown). A nocturnal MCS developed in Wisconsin, propagating east-southeast, with a mature echo signature on radar around 02:30 UTC. This system crossed the barrier islands of Wisconsin at 02:55 UTC and by 03:55 UTC had moved across Lake Michigan, making landfall near Frankfort, MI (FKS). The storm crossed Lake Michigan south of BI; there was associated stratiform rain banding observed to the north of the system, though this remained west of the BIA. Temperature records from the BI airport (SJX) showed no evidence of outflow passage from the system until substantially after the system had crossed the lake. By 05: 00 UTC the leading edge of the decaying bow echo was over the lower peninsula of Michigan (Figure 2).

As the bow echo moved over the Lower Peninsula it produced an outflow boundary which propagated ahead of the system. At Frankfort, MI (FKS, Fig. 2c) a small spike in wind speed and drop in temperature was detected as the MCS made landfall, reflecting passage of an outflow boundary. Further north, this boundary was also observed later propagating 76 miles away at Beaver Island, 90 miles in Port Inland, MI and 116 mi away in Mackinaw City, MI (Fig. 2a,b,d). The arrival of this feature was first detected in surface observations on Beaver Island (SJX, Fig. 2a) where between 05:15 UTC to 06:15 UTC winds rapidly shifted from SW to SSE, while velocity rapidly increased to 16.54 ms^{-1}. Simultaneously, a leading pressure increase of 2.65 hPa was followed by a rapid change with a recorded peak-to-trough decrease of 6.64 hPa. Combined with this pressure change, and despite being in the mid-nocturnal hours, a substantial increase of surface temperature from 69°F to 79° F (20.5° C to 26.1° C) persisted after the pressure

displacement. A temperature increase of this magnitude implies the adiabatic descent of air associated with mixing, which contrasts the typical decrease in temperature seen with outflow boundary passage. Based on these observations, the lack of a storm directly influencing the island, and the presence of a capped boundary layer, this would imply that the feature had transitioned into an atmospheric bore, a type of gravity wave (Wakimoto and Kingsmill 1995), that intensified beyond the weak perturbation seen earlier at FKS. This feature is similar in magnitude to the forcing feature described by Anderson and Mann (2021), albeit with a stronger wind perturbation and no storm present over the island. Given the magnitude of the wind and pressure perturbation generated by this feature is more than sufficient for the generation of a meteotsunami (Bechle et al. 2016), we hypothesize that this event provided the requisite atmospheric forcing.

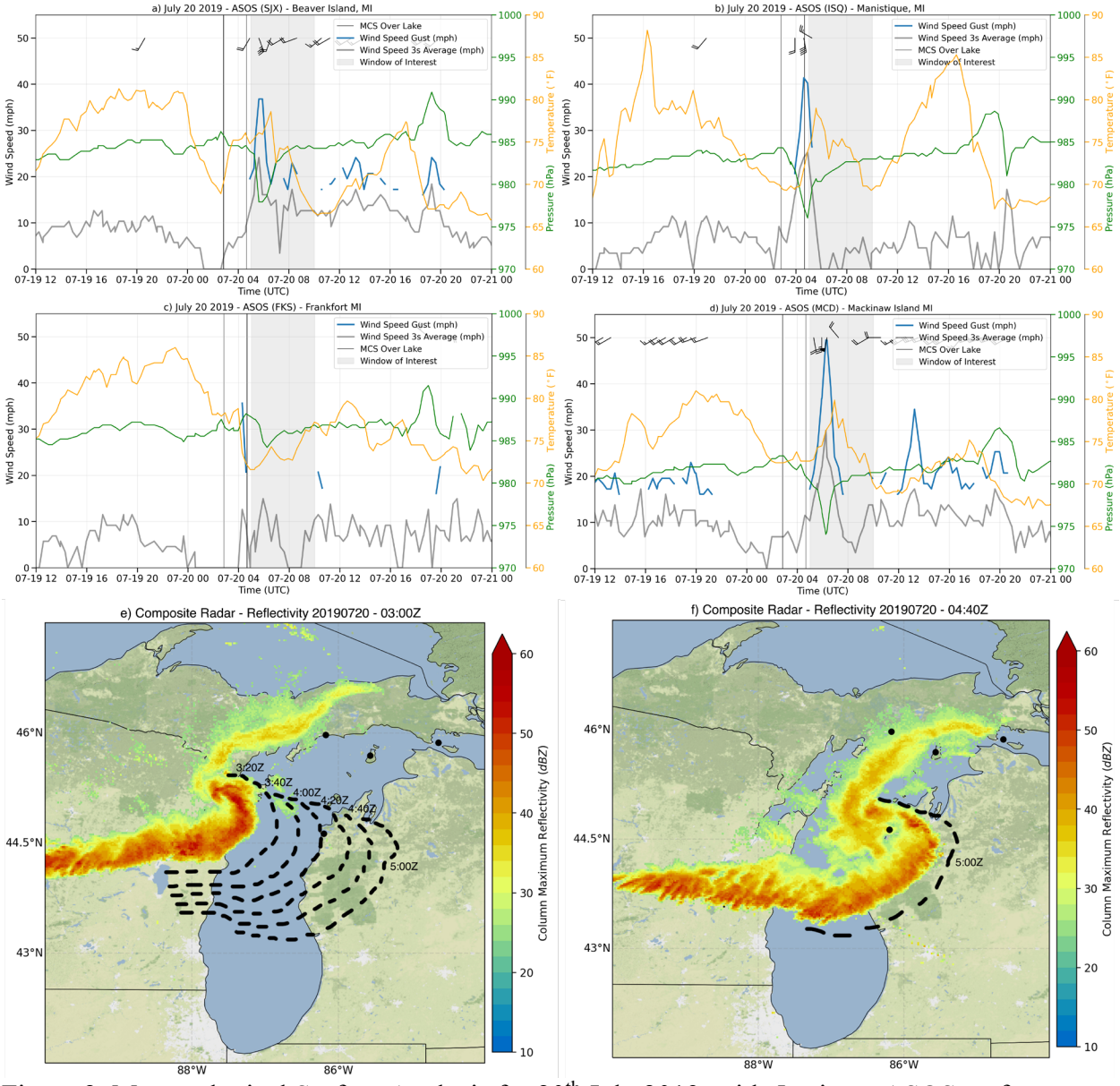

Figure 2. Meteorological Surface Analysis for 20th July 2019, with 5-minute ASOS surface observations and GridRad composite radar. a)-d) Observations from Beaver Island (station SJX),

Manistique (ISQ), Frankfort (FKS), and Mackinaw Island (MCD). Each plot shows 10 m wind speed (grey), wind gust (blue), 2m temperature (gold), and barometric station pressure (green) relative to the period over which storms remain over the lake as depicted in panel e) (red lines). Wind direction in degrees from true north and corresponding wind speed is shown with wind barbs for the periods corresponding to wind gusts. Meteotsunami timing is estimated based on the break point indicated by the analysis shown in Figure 3. e) Maximum column reflectivity at 0300Z on the 20th, with progression of reflectivity leading edge at 20-minute intervals from 0300Z to 0500Z with station locations depicted by the black circles as in Figure 1. f) as for e) except 0440Z on the 20th.

A significant rise (36 cm) in water level beneath the station 1 wetland occurred between 06:30 UTC and 07:30 UTC (Fig. 3); we hypothesize that this was driven by meteotsunami wave action in Sand Bay arising from the documented atmospheric bore. The groundwater level subsequently receded ~25cm in the following hour, returning to a baseline of ~177.8 m asl by 09:00 UTC (Fig. 3). No other substantial hydrologic responses were observed in the subsequent 24 hours after the initial rise and fall described here. The contribution of rainfall to this peak in groundwater levels was ruled out, as rainfall accumulation in the preceding 24 hours was a scant 1.6 mm. The duration and magnitude of the wetland hydrologic response is consistent with what should happen when the system is hit by a single large, short frequency wave, i.e., a (meteo)tsunami.

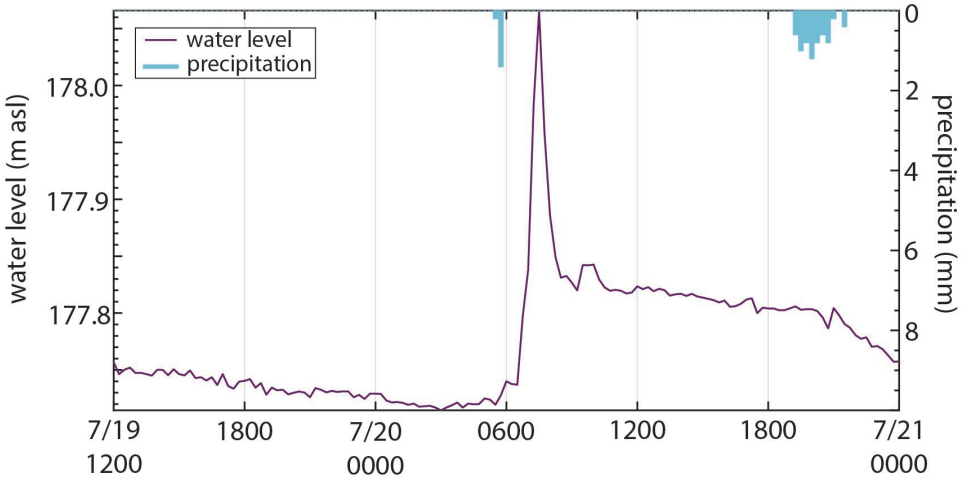

Figure 3. Station 1 wetland groundwater level (0.75m) and precipitation record from 07/19/2019 12:00 UTC – 07/21/2019 0:00 UTC. Note: This event occurred during the time period where stilling well data are unavailable due to equipment failure.

To support our analysis of the observed passage of the meteotsunami impacting the wetland, we analyzed wave action at two surrounding NOS observation stations (Port Inland, MI and Mackinaw City, MI) and conducted a modeling approach analogous to that used by Anderson and Mann (2021). Both Port Inland, MI and Mackinaw City, MI NOS observation stations recorded wave action in the meteotsunami frequency coincident with the observed station 1 wetland response. High frequency wavelets (27.9-minute period) started at 08:42 UTC in the Port Inland record (Fig. 4 b), with a peak wavelet power of 0.156 at 10:36 UTC which had a period of 35.5 minutes and a wavelet power of 23.25*sigma. Meteotsunami waves continued at

Port Inland until 06:00 UTC . Meteotsunami wave action reached Mackinaw City, MI slightly after Port Inland, MI, at 09:36 UTC , with wave periods of 59.7 minutes and a peak wavelet power of 0.065 (6.7 * sigma) at 11:00 UTC . Even higher frequency meteotsunami waves, with periods around 13.4 minutes, started impacting Mackinaw City at 10:36 UTC, with a peak wavelet power of 0.09 (30.4 * sigma) at 11:06 UTC (Fig. 4c). A hydrodynamic simulation of the event further illustrates the presence of meteotsunami activity in the northern end of the lake and specifically near Beaver Island. While the atmospheric forcing used to drive the hydrodynamic model likely exhibits some differences from the realistic conditions as it is driven by a model forecast, to assess this potential difference HRRR forecast data were compared to station observations. This comparison suggests that both windspeeds and pressure tendencies (Figure SI 1) are of a similar magnitude and timing, particularly for the stations close to meteotsunami impact (BJX, ISQ). Given this reliable meteorological forcing, we consider the resulting FVCOM predictions of wave conditions associated with this event (Figures 4a and 5). The initial wave generated by the outflow boundary as MCS crossed can be seen impacting the west coast of Michigan at 02:20 UTC, before propagating northward along the shore toward the BIA over the next hour. Wave heights peak along the coast to the east of the BIA by 03:40 UTC before a series of implied refractions and reflections of waves lead to several wave height peaks in the meteotsunami frequency band (period of approximately 26 minutes, and maximum amplitude of 16 cm) in the vicinity of BIA between 05:30 and 08:00 UTC (Figure 4 and SI 1). While there are no direct observations of the open water around the BIA that can confirm the precise timing of the meteotsunami that produced the surge in the wetlands, these modeling results indicate that there was significant meteotsunami activity in the vicinity of BI station 1 preceding the wetland observation.

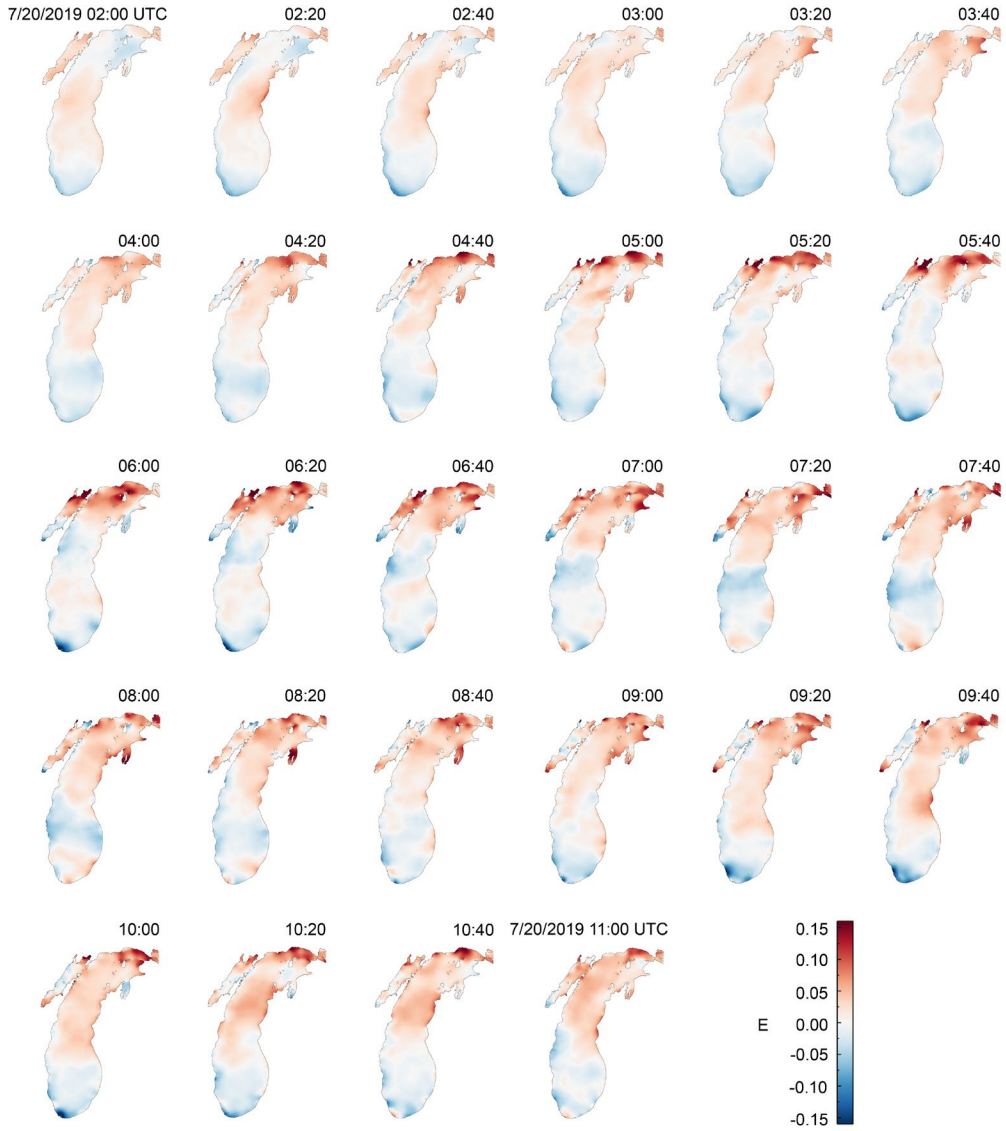

Figure 4. Time lapse images of water surface level on Lake Michigan simulated with the hydrodynamic model for the July 20th, 2019, event.

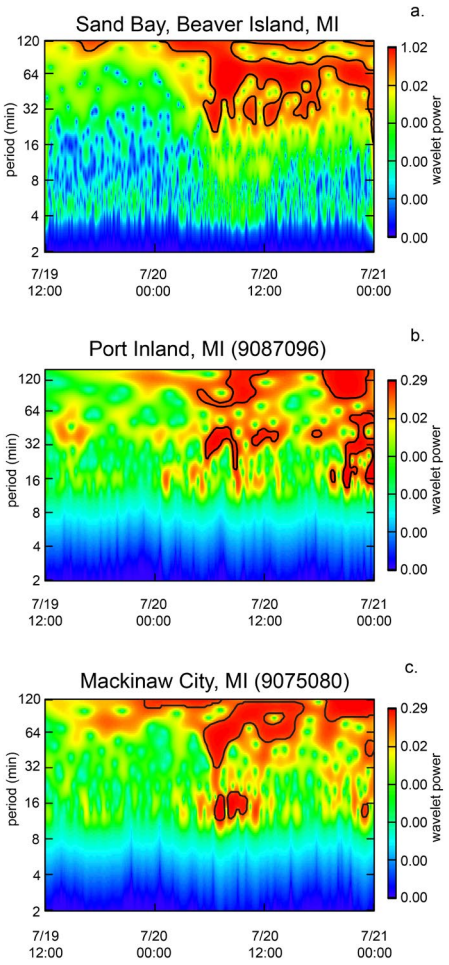

379

380 **Figure 5.** Wavelet analysis for waves in the meteotsunami periodicity range of 2-120 minutes
381 from a. Sand Bay, Beaver Island, MI (FVCOM model output), b. Port Inland, MI (NOS ID
382 9087096), and c. Mackinaw City, MI (NOS ID 9075080). The black lines on the wavelet
383 analysis images indicate the times where wavelet power was > 6*sigma. All times are in UTC.

384 **5 Discussion**

385 The clear and pronounced wetland response documented in the July 20th case highlights
386 what we hypothesize is close to the idealized response of an incipient foredune/swale wetland to
387 meteotsunami influence. In this simple case (single meteorological forcing and negligible
388 precipitation) we illustrate wetland hydrologic dynamics in response to disturbance via
389 meteotsunami eventsby linking the wetland hydrologic response to co-occurring meteotsunami
390 waves hitting lake level observation stations in the region, identifying the atmospheric driver for
391 meteotsunami formation, in this case the undular bore, and simulating meteotsunami generation
392 at the wetland site just before the observed hydrologic response through a hydrodynamic model.
393 By using these four separate lines of evidence we present a compelling case for linking the
394 wetland hydrologic response to meteotsunami influence. The meteotsunami literature to-date has
395 not identified what meteotsunami influence might look like in an incipient foredune/swale
396 wetland, thus we present this case as a basis for future wetland comparisons. Established
397 methods for detecting meteotsunami in water level records fail in these kinds of systems because

1) they rely on methods that assume symmetry in rising and falling limbs of the hydrograph, which is not the case in the response of an isolated wetland such as we examined here (Fig 2. a), and 2) the propagation of pressure waves through porous media elongates, filters, and attenuates the meteotsunami signal, making the hydrologic effect(s) more difficult to distinguish. The challenges with identifying meteotsunami influence in isolated wetlands become even more apparent when the events influencing the wetland are compounded with precipitation signals , seiche, storm surge, reflection/refraction of waves from an initial meteotsunami event, and/or multiple meteotsunami events occurring back-to-back (as occurred during other probable meteotsunami events captured in this wetland's record not discussed here).

The type and timing of the meteorological forcing that generated the meteotsunami event documented here also highlight both the novelty of this case and some potential limitations of existing methodology and understanding of system interactions. While bores and other forms of atmospheric gravity waves have recently been hypothesized (Bechle et al. 2016) and demonstrated (for directly forced internal gravity waves; Anderson and Mann 2021) to cause meteotsunamis in the Great Lakes, we can show that in the July 20th case an atmospheric bore far away from the convective feature was the forcing that generated the meteotsunami observed in both the NOS and wetland water levels. In contrast to the results of Linares et al. (2016) and Anderson and Mann (2021), both pressure and wind related stresses from the bore likely contributed to meteotsunami formation, despite the convective origin of the storm event. This suggests that situations producing bores may lead to meteotsunamis that are remote of the convective forcing.

The data presented in this study reflect a single incipient foredune/swale wetland system during a period of above average lake levels. Therefore, we are limited in our ability to quantify meteotsunami influence from our existing data as the station 1 wetland had no capability to record lake level, requiring us to rely on distant NOAA NOS gauges and gridded output from hydrodynamic models. This provides challenges for analysis of travel times, directionality, reflection/refraction, and estimates of tsunami runup as we are comparing datasets with different distances from meteotsunami origin, coastline shapes, and bathymetries, as well as limitations in the accuracy of numerical weather forcing, hydrodynamic model physics, and topographic and bathymetric representation. A recent meteotsunami study has illustrated the sensitivity of meteotsunami simulations to shoreline resolution, which can impact wave amplitude and period (Huang et al., 2021). Additionally, we note there is insufficient information about how wetland systems beyond our studied location may respond to differing event magnitude, coastline shape, nearshore bathymetry, and lake levels. Because much of the previous research into meteotsunamis has focused on destructive events in populated regions, there is a significant knowledge gap surrounding the interaction between these events and protected wetlands. Potentially interesting and valuable phenomena may be overlooked as a result. The role of meteotsunami events in the hydrologic response, sediment budget, and system dynamics of incipient foredune/swale wetlands should be investigated further as these features often form the first line of defense for a resilient coastline. Subsurface water levels and retention can have substantial impact on the vegetation regime, nutrient cycling, and sediment stability of foredune-swale type wetlands (e.g., Albert et al. 2005; Skalbeck et al. 2009; Leira et al. 2019 and others) and the influence of meteotsunami events on water availability, salinity (in the case of wetlands adjacent to seawater), and hydrogeomorphic evolution is a topic that merits further consideration.

6 Conclusions

Here we report a case study analysis of a unique dataset recording the hydrologic response of an isolated wetland on Beaver Island in northern Lake Michigan to meteotsunami influence. We documented large, sharp deviations in wetland water levels coincident with meteotsunami waves striking regional NOAA NOS stations in northern Lake Michigan, hydrodynamic model output indicating meteotsunami wave generation in northern Lake Michigan, and analyzed atmospheric data to identify the likely causes of the meteotsunami events. The case in this study documents influence of meteotsunamis on the hydrologic response of isolated wetlands, demonstrate the range of meteotsunami-generating atmospheric forcing, highlight limitations of current methodology (i.e. the identification of meteotsunami events through wetland hydrologic records, and prediction of meteotsunami forming phenomena) and provide compelling evidence to support future research in this area. While this study was limited to a single wetland located in northern Lake Michigan, the outcomes documented here have implications for nearshore isolated wetlands along coastal regions vulnerable to meteotsunami events.

Acknowledgments, Samples, and Data

The authors have no conflicts of interest to declare. The data unique to this study (wetlands observations) are available as a .csv file on Hydroshare (https://doi.org/10.4211/hs.3b81222420c448de862ab16a109cd8d7). All other data sources used are publicly available from their respective repositories. Funding for this work was provided to Drs. Robertson and Kluver through a seed grant from Central Michigan University's Institute for Great Lakes Research (IGLR). The authors would like to thank Cody Converse, Kyle Delong, Alison Veresh, and Matt Werle for assistance with installation and maintenance of field equipment. We would also like to thank the CMU Biological Station, IGLR staff, Dr. Don Uzarski and Rachael Agardy for their assistance as well. Thank you to the editors and reviewers for your feedback and comments that help to improve the final product. This paper is Contribution Number XXXX of the Central Michigan University Institute for Great Lakes Research.

References

Albert, D.A., Wilcox, D.A, Ingram, J.W., & Thompson, T.A. (2005). Hydrogeomorphic Classification for Great Lakes Coastal Wetlands. *Journal of Great Lakes Research (31)*1, 129-146. https://doi.org/10.1016/S0380-1330(05)70294-X

Anarde, K., Cheng, W., Tissier, M., Figlus, J., & Horrillo, J. (2021). Meteotsunamis Accompanying Tropical Cyclone Rainbands During Hurricane Harvey. *Journal of Geophysical Research: Oceans*, *126*(1), e2020JC016347. https://doi.org/10.1029/2020JC016347

Anderson, E. J., & Mann, G. E. (2021). A high-amplitude atmospheric inertia–gravity wave-induced meteotsunami in Lake Michigan. *Natural Hazards*, *106*(2), 1489–1501. https://doi.org/10.1007/s11069-020-04195-2

Anderson, E.J., Bechle, A.J., Wu, C.H., Schwab, D.J., Mann, G.E., & Lombardy, K.A. (2015). Reconstruction of a meteotsunami in Lake Erie on 27 May 2012: Roles of atmospheric conditions on hydrodynamic response in closed basins. *Journal of Geophysical Research: Oceans* (120)12 8020-8038. https://doi.org/10.1002/2015JC010883

Anderson EJ, Fujisaki-Manome A, Kessler J, Lang GA, Chu PY, Kelley JGW, Chen Y, & Wang J (2018) Ice forecasting in the next-generation Great Lakes Operational Forecast System (GLOFS). J Mar Sci Eng 6(4):123. https://doi.org/10.3390/jmse6040123

Anderson E.J. & Schwab D.J. (2013) Predicting the oscillating bi-directional exchange flow in the Straits of Mackinac. J Great Lakes Res 39(4):66671

Anderson E.J. & Schwab D.J. (2017) Meteorological influence on summertime baroclinic exchange in the Straits of Mackinac. J Geophys Res Oceans 122(3):2171–2182

Angove, M., Kozlosky, L., Chu, P., Dusek, G., Mann, G., Anderson, E., et al. (2021). Addressing the meteotsunami risk in the united states. *Natural Hazards*, *106*(2), 1467–1487. https://doi.org/10.1007/s11069-020-04499-3

Barbier, E. B. (2013). Valuing Ecosystem Services for Coastal Wetland Protection and Restoration: Progress and Challenges. *Resources*, *2*(3), 213–230. https://doi.org/10.3390/resources2030213

Bechle, A. J., & Wu, C. H. (2015). The Lake Michigan meteotsunamis of 1954 revisited. In I. Vilibić, S. Monserrat, & A. B. Rabinovich (Eds.), *Meteorological Tsunamis: The U.S. East Coast and Other Coastal Regions* (pp. 155–177). Cham: Springer International Publishing. https://doi.org/10.1007/978-3-319-12712-5_9

Bechle, A. J., Kristovich, D. A. R., & Wu, C. H. (2015). Meteotsunami occurrences and causes in Lake Michigan. *Journal of Geophysical Research: Oceans*, *120*(12), 8422–8438. https://doi.org/10.1002/2015JC011317

Bechle, A. J., Wu, C. H., Kristovich, D. A. R., Anderson, E. J., Schwab, D. J., & Rabinovich, A. B. (2016). Meteotsunamis in the Laurentian Great Lakes. *Scientific Reports*, *6*(1), 37832. https://doi.org/10.1038/srep37832

Benjamin SG, Weygandt SS, Brown JM, Hu M, Alexander CR, Smirnova TG, Olson JB, James EP, Dow- ell DC, Greg GA, Lin H, Peckham SE, Smith TL, Moninger WR, Kenyon JS, Manikin GS (2016) A North American hourly assimilation and model forecast cycle: the rapid refresh. Mon Weather Rev 144:1669–1694. https://doi.org/10.1175/MWR-D-15-0242.1

Bowman, K. P., and C. R. Homeyer (2017), GridRad - Three-Dimensional Gridded NEXRAD WSR-88D Radar Data, https://doi.org/10.5065/D6NK3CR7, Research Data Archive at the National Center for Atmospheric Research, Computational and Information Systems Laboratory, Boulder, Colo. (Updated irregularly.) Accessed 07/07/2021.

ten Brink, U. S., Chaytor, J. D., Geist, E. L., Brothers, D. S., & Andrews, B. D. (2014). Assessment of tsunami hazard to the U.S. Atlantic margin. *Marine Geology*, *353*, 31–54. https://doi.org/10.1016/j.margeo.2014.02.011

Carmona, R., Hwang, W.-L., & Torresani, B. (1998). *Practical Time-Frequency Analysis: Gabor and Wavelet Transforms, with an Implementation in S*. Academic Press.

Cooney, J. W., Bowman, K. P., Homeyer, C. R., & Fenske, T. M. (2018). Ten Year Analysis of Tropopause-Overshooting Convection Using GridRad Data. *Journal of Geophysical Research: Atmospheres*, *123*(1), 329–343. https://doi.org/10.1002/2017JD027718

Chen C, Beardsley RC, Cowles G (2006) An unstructured grid, finite volume coastal ocean model (FVCOM) system. Oceanography 19:78–89

Curreli, A., Wallace, H., Freeman, C., Hollingham, M., Stratford, C., Johnson, H., & Jones, L. (2013). Eco-hydrological requirements of dune slack vegetation and the implications of climate change. *Science of The Total Environment*, *443*, 910–919. https://doi.org/10.1016/j.scitotenv.2012.11.035

Dusek, G., DiVeglio, C., Licate, L., Heilman, L., Kirk, K., Paternostro, C., & Miller, A. (2019). A Meteotsunami Climatology along the U.S. East Coast. *Bulletin of the American Meteorological Society*, *100*(7), 1329–1345. https://doi.org/10.1175/BAMS-D-18-0206.1

Ewing, M., Press, F., & Donn, W.L. (1954). An explanation of the Lake Michigan Wave of 26 June 1954. *Science* (120)3122 684-686. DOI: 10.1126/science.120.3122.684

Farrand, W. R., & Bell, D. L. (1982). Quaternary Geology of Michigan (map). Michigan Department of Natural Resources - Geological Survey.

Girdler, E. B., & Connor Barrie, B. T. (2008). The scale-dependent importance of habitat factors and dispersal limitation in structuring Great Lakes shoreline plant communities. *Plant Ecology*, *198*(2), 211–223. https://doi.org/10.1007/s11258-008-9396-z

Gracia, A., Rangel-Buitrago, N., Oakley, J. A., & Williams, A. T. (2018). Use of ecosystems in coastal erosion management. *Ocean & Coastal Management*, *156*, 277–289. https://doi.org/10.1016/j.ocecoaman.2017.07.009

Gusiakov, V. K. (2021). Meteotsunamis at global scale: problems of event identification, parameterization and cataloguing. *Natural Hazards: Journal of the International Society for the Prevention and Mitigation of Natural Hazards*, *106*(2), 1105–1123. Retrieved from https://ideas.repec.org/a/spr/nathaz/v106y2021i2d10.1007_s11069-020-04230-2.html

Haberlie, A. M., & Ashley, W. S. (2019). A Radar-Based Climatology of Mesoscale Convective Systems in the United States. *Journal of Climate*, *32*(5), 1591–1606. https://doi.org/10.1175/JCLI-D-18-0559.1

Homeyer, C. R., & Bowman, K.P. (2017). Algorithm Description Document for Version 3.1 of the Three-Dimensional Gridded NEXRAD WSR-88D Radar (GridRad) Dataset, Technical Report.

Huang, C., Anderson, E., Liu, Y., Ma, G., Mann, G., & Xue, P. (2021). Evaluating essential processes and forecast requirements for meteotsunami-induced coastal flooding. Natural Hazards, 110, 1693-1718 (2022). https://doi.org/10.1007/s11069-021-05007-x

Kelly, D. L., Schaefer, J. T., & Doswell, C. A. (1985). Climatology of Nontornadic Severe Thunderstorm Events in the United States. *Monthly Weather Review*, *113*(11), 1997–2014. https://doi.org/10.1175/1520-0493(1985)113<1997:CONSTE>2.0.CO;2

Lagerquist, R., Allen, J. T., & McGovern, A. (2020). Climatology and Variability of Warm and Cold Fronts over North America from 1979 to 2018. *Journal of Climate*, *33*(15), 6531–6554. https://doi.org/10.1175/JCLI-D-19-0680.1

Laird, N. F., Kristovich, D. A. R., Liang, X.-Z., Arritt, R. W., & Labas, K. (2001). Lake Michigan Lake Breezes: Climatology, Local Forcing, and Synoptic Environment. *Journal of Applied Meteorology and Climatology*, *40*(3), 409–424. https://doi.org/10.1175/1520-0450(2001)040<0409:LMLBCL>2.0.CO;2

Leira, M., Freitas, M.C., Ferriera, T., Cruces, A., Connor, S., Andrade, C., Lopes, V., & Bao, R. (2019). Holocene sea level and climate interactions on wet dune slack evolution in SW Portugal: A model for future scenarios? *The Holocene,* (29)1,, 26-44. https://doi.org/10.1177/0959683618804633

571 Linares, Á., Bechle, A. J., & Wu, C. H. (2016). Characterization and assessment of the
572 meteotsunami hazard in northern Lake Michigan. *Journal of Geophysical Research:*
573 *Oceans*, *121*(9), 7141–7158. https://doi.org/10.1002/2016JC011979
574 Linares, Á., Wu, C. H., Anderson, E. J., & Chu, P. Y. (2018). Role of Meteorologically Induced
575 Water Level Oscillations on Bottom Shear Stress in Freshwater Estuaries in the Great
576 Lakes. *Journal of Geophysical Research: Oceans*, *123*(7), 4970–4987.
577 https://doi.org/10.1029/2017JC013741
578 Linares, Á., Wu, C. H., Bechle, A. J., Anderson, E. J., & Kristovich, D. A. R. (2019).
579 Unexpected rip currents induced by a meteotsunami. *Scientific Reports*, *9*(1), 2105.
580 https://doi.org/10.1038/s41598-019-38716-2

581 Lorenz, E.U. (1972). Lecture on Predictability: Does the Flap of a Butterfly's Wings in Brazil
582 Set off a Tornado in Texas? Massachusetts Institute of Technology, Cambridge.
583 Matheny, K. (2017, June 19). Tsunamis? On the Great Lakes? They happen — sometimes with
584 deadly results. *Detroit Free Press*. Retrieved from
585 https://www.freep.com/story/news/local/michigan/2017/06/19/great-lakes-
586 tsunamis/408563001/
587 Michigan Department of Environmental Quality. (1987). Bedrock Geology of Michigan
588 1:500,000-Scale. Retrieved from https://catalog.data.gov/dataset/bedrock-geology-of-
589 michigan-1-500000-scale
590 Monserrat, S., Vilibić, I., & Rabinovich, A. B. (2006). Meteotsunamis: atmospherically induced
591 destructive ocean waves in the tsunami frequency band. *Natural Hazards and Earth*
592 *System Sciences*, *6*(6), 1035–1051. https://doi.org/10.5194/nhess-6-1035-2006

593 National Geophysical Data Center (1996). Bathymetry of Lake Michigan. National Geophysical
594 Data Center, NOAA. doi:10.7289/V5B85627 [accessed July 2021].

595 National Oceanic and Atmospheric Administration, National Aeronautics and Space
596 Administration, and U. S. Air Force (1976). U. S. Standard Atmosphere 1976, U.S.
597 Government Printing Office, Washington, DC.

598 National Oceanographic and Atmospheric Administration, 1998: Automated Surface Observing
599 System User's Guide. Last Accessed: 3/4/2022 URL:
600 https://www.weather.gov/media/asos/aum-toc.pdf
601 Nomitsu, T. (1935). A theory of tsunamis and seiches produced by wind and barometric gradient.
602 Mem Coll Sci Kyoto Imp Univ 18:201–214

603 Pattiaratchi, C., & Wijeratne, E. M. S. (2014). Observations of meteorological tsunamis along
604 the south-west Australian coast. *Natural Hazards*, *74*(1), 281–303.
605 https://doi.org/10.1007/s11069-014-1263-8
606 Pattiaratchi, C. B., & Wijeratne, E. M. S. (2015). Are meteotsunamis an underrated hazard?
607 *Philosophical Transactions. Series A, Mathematical, Physical, and Engineering Sciences*,
608 *373*(2053), 20140377. https://doi.org/10.1098/rsta.2014.0377

Peng, M., A. Zhang, E.J. Anderson, G.A. Lang, J.G.W. Kelley, Y. Chen (2019). Implementation of the Lakes Michigan and Huron Operational Forecast System (LMHOFS) and the nowcast/forecast skill assessment, NOAA Technical Report NOS CO-OPS 091.

Platzman, G. (1958). *A numerical computation of the storm surge of 26 June 1954 on Lake Michigan* (No. 1). Tech. Rep.

Rabinovich, A. B., Thomson, R. E., & Stephenson, F. E. (2006). The Sumatra tsunami of 26 December 2004 as observed in the North Pacific and North Atlantic oceans. *Surveys in Geophysics*, *27*(6), 647–677. https://doi.org/10.1007/s10712-006-9000-9

Roesch, A. & Schmidbauer, H. (2018). WaveletComp: Computational Wavelet Analysis. R package version 1.1. https://CRAN.R-project.org/package=WaveletComp

Sanders, F., & Hoffman, E. G. (2002). A Climatology of Surface Baroclinic Zones. *Weather and Forecasting*, *17*(4), 774–782. https://doi.org/10.1175/1520-0434(2002)017<0774:ACOSBZ>2.0.CO;2

Skalbeck, J.D., Reed, D.M., Hunt, R.J. & Lambert, J.D. (2009). Relating groundwater to seasonal wetland in southeastern Wisconsin, USA. *Hydrogeology Journal* (17) 215-228. https://doi.org/10.1007/s10040-008-0345-7

Smithsonian Institution & List, Robert J. (1951). Smithsonian meteorological tables *Smithsonian Miscellaneous Collections*, **144**, 151 pp.

Sous, D., Lambert, A., Michallet, H., & Rey, V. (2011). Groundwater pressure dynamics in a laboratory swash zone. *Journal of Coastal Research*, 2074–2078. Retrieved from https://www.jstor.org/stable/26482541

Taszarek, M., Allen, J. T., Groenemeijer, P., Edwards, R., Brooks, H. E., Chmielewski, V., & Enno, S.-E. (2020). Severe Convective Storms across Europe and the United States. Part I: Climatology of Lightning, Large Hail, Severe Wind, and Tornadoes. *Journal of Climate*, *33*(23), 10239–10261. https://doi.org/10.1175/JCLI-D-20-0345.1

Taszarek, M., Allen, J. T., Púčik, T., Hoogewind, K. A., & Brooks, H. E. (2020). Severe Convective Storms across Europe and the United States. Part II: ERA5 Environments Associated with Lightning, Large Hail, Severe Wind, and Tornadoes. *Journal of Climate*, *33*(23), 10263–10286. https://doi.org/10.1175/JCLI-D-20-0346.1

Torrence C., & Compo G.P. (1998). A practical guide to wavelet analysis. Bulletin of the American Meteorological Society 79 (1), 61–78.

USDA-FSA-APFO Aerial Photography Field Office (2010). FSA 10:1 NAIP Imagery m_4508520_ne_16_1_20100801 3.75 x 3.75 minute JPEG2000 from The National Map: USDA-FSA-APFO Aerial Photography Field Office.

USDA-FSA-APFO Aerial Photography Field Office (2014). FSA 10:1 NAIP Imagery m_4508520_ne_16_1_20140916 3.75 x 3.75 minute JPEG2000 from The National Map: USDA-FSA-APFO Aerial Photography Field Office.

USDA-FSA-APFO Aerial Photography Field Office (2020). FSA 10:1 NAIP Imagery m_4508520_ne_16_1_20200728 3.75 x 3.75 minute JPEG2000 from The National Map: USDA-FSA-APFO Aerial Photography Field Office.

U.S. Geological Survey (2020). USGS one meter x61y507 MI Charlevoix Islands 2016: U.S. Geological Survey.

Vilibić, I., Šepić, J., Rabinovich, A. B., & Monserrat, S. (2016). Modern Approaches in Meteotsunami Research and Early Warning. *Frontiers in Marine Science*, *3*. https://doi.org/10.3389/fmars.2016.00057

Vilibić, I., Rabinovich, A. B., & Anderson, E. J. (2021). Special issue on the global perspective on meteotsunami science: editorial. *Natural Hazards*, *106*(2), 1087–1104. https://doi.org/10.1007/s11069-021-04679-9

652 Waddell, E. (1987). Swash-Groundwater-Beach profile interactions. *In* Davis, R.A., Etherington,
653 R.L. (eds.) *Beach and Nearshore Sedimentation*. SEPM Special Publication, 24, 1
654 15-125.
655 Williams, D. A., Schultz, D. M., Horsburgh, K. J., & Hughes, C. W. (2021). An 8-yr
656 Meteotsunami Climatology across Northwest Europe: 2010–17. *Journal of Physical*
657 *Oceanography*, *51*(4), 1145–1161. https://doi.org/10.1175/JPO-D-20-0175.1
658 Zedler, J. B., & Kercher, S. (2005). WETLAND RESOURCES: Status, Trends, Ecosystem
659 Services, and Restorability. *Annual Review of Environment and Resources*, *30*(1), 39–74.
660 https://doi.org/10.1146/annurev.energy.30.050504.144248
661